HHS Public Access

Author manuscript

Angew Chem Int Ed Engl. Author manuscript; available in PMC 2022 May 17.

Published in final edited form as:

Angew Chem Int Ed Engl. 2021 May 17; 60(21): 12007–12012. doi:10.1002/anie.202100774.

Reversible Ratiometric NADH Sensing Using Semiconducting Polymer Dots

Haobin Chen[a], **Jiangbo Yu**[a], **Xiaoxiao Men**[b], **Jicheng Zhang**[a], **Zhaoyang Ding**[a], **Yifei Jiang**[a], **Changfeng Wu**[b], **Daniel T. Chiu**[a],*

[a]Department of Chemistry and Bioengineering, University of Washington, Seattle, WA, 98195, USA

[b]Department of Biomedical Engineering, Southern University Science and Technology, Shenzhen, Guangdong, 510855, China

Abstract

Reduced nicotinamide adenine dinucleotide (NADH) is a key coenzyme in living cells due to its role as an electron carrier in redox reactions, and its concentration is an important indicator of cell metabolic state. Abnormal NADH levels are associated with age-related metabolic diseases and neurodegenerative disorders, creating a demand for a simple, rapid analytical method for point-of-care NADH sensing. Here we develop a series of NADH-sensitive semiconducting polymer dots (Pdots) as nanoprobes for NADH measurement, and test their performance *in vitro* and *in vivo*. NADH sensing is based on electron transfer from semiconducting polymer chains in the Pdot to NADH upon UV excitation, quenching Pdot fluorescence emission. In polyfluorene-based Pdots, this mechanism resulted in an on-off NADH sensor; in DPA-CNPPV Pdots, UV excitation resulted in NADH-sensitive emission at two wavelengths, enabling ratiometric detection. Ratiometric NADH detection using DPA-CNPPV Pdots exhibits high sensitivity (3.1 μM limit of detection), excellent selectivity versus other analytes, reversibility, and a fast response (less than 5 s). We demonstrate applications of the ratiometric NADH-sensing Pdots including smartphone-based NADH imaging for point-of-care use.

Graphical Abstract

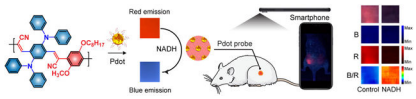

A simple, rapid analytical method for NADH sensing is achieved by electron transfer from a Pdot to NADH upon UV excitation. Ratiometric NADH detection using DPA-CNPPV Pdots exhibits high sensitivity, excellent selectivity versus other analytes, and a fast and reversible response. Smartphone-based *in vivo* ratiometric imaging of NADH is performed to demonstrate the feasibility of point-of-care use.

*Corresponding author. chiu@uw.edu.

Conflict of Interest

J.Y. and D.T.C. have a financial interest in Lamprogen, which has licensed the described technology from the University of Washington.

Keywords

semiconducting polymer dots (Pdots); reduced nicotinamide adenine dinucleotide (NADH); ratiometric sensor; smartphone biosensor

Introduction

The NAD^+/NADH redox couple is essential in cell metabolism, acting as a coenzyme for over 500 NAD-dependent enzymes.[1, 2] The ratio of NAD^+ to NADH concentration is an important indicator of cell metabolic state,[3, 4] and changes in NAD^+ and NADH concentrations are associated with embryonic development, calcium homeostasis, cell death, and aging, and with diseases such as cancer, epilepsy, and Parkinson's disease.[5–9] Probes that can rapidly and accurately measure NAD^+ and NADH concentration at the point of care are desirable to improve disease diagnosis and management. Current methods to quantify NAD^+ and NADH such as chromatography, colorimetry, mass spectrometry, fluorescence lifetime, and assays involving fluorescent proteins and enzymatic cycling[3, 10–13] are unsuitable for *in situ* point-of-care measurements due to their complexity and high equipment costs, or are limited by low sensitivity and selectivity. New methods that can accurately quantify NAD^+ and NADH in a point-of-care setting are needed.

Semiconducting polymer dots (Pdots) are fluorescent nanoparticles[14–17] that exhibit superior photophysical properties relative to small fluorophores, inorganic semiconducting quantum dots, and fluorescent proteins. Pdots exhibit high brightness, fast emission, large absorption cross-section, and high photostability, as well as low toxicity and versatile surface modification,[18–21] making them well-suited for applications in cell labeling,[22] *in vivo* imaging,[23,24] single-particle tracking,[25] drug/gene delivery,[26] and tumor therapy.[27] Pdots also have been used as biosensors[28,29] to detect pH,[30–31] temperature,[32] metal ions,[33] oxygen,[34] glucose,[35–36] and exosomes.[37]

Here we design a series of NADH-responsive Pdots for use as an NADH sensor, and characterize the Pdots *in vitro* and *in vivo*. NADH sensing is achieved by electron transfer from a Pdot to NADH, resulting in quenching of Pdot fluorescence emission. In polyfluorene-based Pdots this mechanism results in on-off NADH sensing; in DPA-CNPPV Pdots, UV excitation causes NADH-sensitive emission at two wavelengths, enabling ratiometric detection with high sensitivity, excellent selectivity versus other analytes, and a fast, reversible response. We demonstrate the feasibility of point-of-care measurements by performing *in vivo* ratiometric NADH imaging with a smartphone.

Results and Discussion

Synthesis and characterization of NADH-sensitive Pdots

We created a series of NADH-sensitive Pdots with fluorescence emissions spanning the visible spectrum by using the semiconducting polymers PFO, PDHF, PFBT, PFBTTBT, PFTBT (structures in Figure S1), and DPA-CNPPV (poly[{2-methoxy-5-(2-ethylhexyloxy)-1,4-(1-cyanovinylenephenylene)}-co-{2,5-bis(N,N'-diphenylamino)-1,4-phenylene}]; structure in Scheme 1a). The Pdots were prepared by nanoprecipitation

methods we developed previously[14, 22] in which Pdot formation is driven by hydrophobic interactions between a fluorescent semiconducting polymer and the amphiphilic polymer poly(styrene-co-maleic anhydride) (PSMA).

The six Pdots were approximately spherical based on transmission electron microscopy (TEM), with average hydrodynamic diameters in the range of 17.5–22.1 nm (Figure 1a, b; Table 1). All Pdots had a negatively charged surface at neutral pH, with an initial ζ-potential ranging from −38.5 to −36.2 mV (Figure 1c). The Pdots remained stable for four weeks in phosphate-buffered saline (PBS) at room temperature with no apparent aggregation or decomposition (Figure S2). Pdot absorption and emission properties vary depending on the semiconducting polymer structure. Under UV illumination, the emissions of the Pdot suspensions were intense and spanned the visible spectrum (Figure 1d). Pdot absorption and emission are shown in Figure 1e, f.

Fluorescence response of Pdots to NADH in solution

We first examined the fluorescence response of the polyfluorene-based Pdots (PFO, PDHF, PFBT, PFBTTBT, and PFTBT) to NADH in water. The fluorescence emission spectra of the polyfluorene Pdots changed significantly over the range of 0–10 mM NADH with excitation of fluorene groups (Figure 2a–e). Fluorescence emission was quenched at higher NADH. In living cells, some NAD^+ is phosphorylated to $NADP^+$ and converted to NADPH, an electron acceptor similar to NADH. We observed similar Pdot responses to NADPH as to NADH (Figure S3).

Stern-Volmer plots of the ratio of Pdot fluorescence emission intensity at the peak emission wavelength in the absence (F_0) and presence (F) of NADH showed a linear response over the physiological range of NADH (0–2 mM) (Figure 2f, Figure S4). The limit of detection (LOD) ranged from 14 μM for PFBT Pdots to 36 μM for PDHF Pdots. Quenching constants (K_{SV}) ranged from 0.94×10^3 M^{-1} for PDHF to 4.89×10^3 M^{-1} for PFBT (Table 1). PFBT Pdots exhibited the smallest LOD and largest K_{SV}, indicating the highest sensitivity, and were selected for use in subsequent experiments. Table 1 lists the photophysical properties of the polyfluorene-based and DPA-CNPPV Pdots.

We hypothesize that UV absorption by fluorene or triphenylamino group results in formation of electrons in the polymer chains that are transfer to NADH (Figure S5), a reduced form of the coenzyme and which can serve as a high-energy electron transporter,[38,39] This process involves electron diffusion along the polymer chain and results in formation of hole polarons that quench Pdot emission.[40, 41] These results demonstrate that Pdots can function as on/off probes for NADH detection.

Ratiometric probes can provide greater accuracy and sensitivity than on/off probes because ratiometric sensing involves an internally calibrated signal.[42–44] To create a ratiometric probe, we prepared Pdots with DPA-CNPPV (Scheme 1). The triphenylamino structure of bis(diphenylamino)benzene in DPA is a strong electron-donating group with good hole-transporting mobility and an absorption peak at 297 nm. In the presence of NADH, UV illumination of DPA-CNPPV Pdots results in the transfer of electrons in bis(diphenylamine)benzene to nearby NADH to quench the emission of CNPPV. NADH in

solution has a blue emission with a peak at 458 nm. Unlike PFBT Pdots, DPA-CNPPV Pdots have little absorption in the blue region, so there is little energy transfer from NADH to DPA-CNPPV Pdots (Figure S6). The DPA-CNPPV Pdots exhibit an emission maximum at 627 nm when excited at 385 nm; addition of NADH caused a large decrease in emission at 627 nm and a concomitant increase at 458 nm with increasing NADH over its physiological range (0–2 mM) (Figure 3a) and at higher concentrations (2–50 mM) (Figure 3c). This Pdot thus functions as a ratiometric NADH sensor. The sensitivity of the ratiometric probe was as high as 2.89×10^5 M^{-1} within the physiological range of 0–2 mM NADH. The fluorescence quantum yield (QY) over the range of 500–800 nm was reduced from 10.8% to 3.4% by adding 100 mM NADH. The emission intensity ratio $R = I_{458nm}/I_{627nm}$ increased linearly with NADH concentration from 0–10 mM (Figure 3b, d). This dynamic range is larger than that of other NADH-sensitive fluorescent materials such as quantum dots, dye molecules, metal complexes, and fluorescent proteins (Table S1). The LOD of NADH was 3.1 μM when using the DPA-CNPPV Pdots, a much lower LOD than when using the five polyfluorene Pdots (14–36 μM LOD).

The fluorescence intensity of the DPA-CNPPV Pdots remained constant under continuous illumination at 385 nm for 30 min, indicating excellent photostability (Figure 3e). The fluorescence response to addition of NADH was rapid (less than 5 s, limited by mass transfer) (Figure 3f), consistent with an electron transfer mechanism. Addition of NADH (1 mM) triggered a large change in emission, whereas no change in emission was observed upon addition of 10 other analytes--oxidizing and reducing species (H_2O_2, NAD^+), carbohydrate derivatives (glucose, lactate, citrate), and abundant cellular cations (Na^+, K^+, Mg^{2+}, Ca^{2+}, Cl^-) at 1 mM (Figure 3g, h), indicating selectivity for NADH. We also tested the potential effect of flavin adenine dinucleotide (FAD) and its reduced form $FADH_2$ on the Pdot sensor. FAD is fluorescent with an emission maximum at 526 nm; $FADH_2$ is non-fluorescent. FAD had no significant effect on Pdot fluorescence in the concentration range of 0–10 μM FAD (Figure S7), a range that extends well above the physiological range of FAD (0.04–0.1 μM). [45,46]

To test the reversibility of the response, the DPA-CNPPV Pdots were exposed repeatedly to 0 and 1 mM NADH by ultrafiltration and gel filtration. The Pdot fluorescence response remained unchanged over six measurement cycles (Figure 3i), demonstrating excellent reversibility, consistent with a mechanism involving electron transfer without a chemical reaction.

Detecting NADH in live cells

We next applied the Pdots to imaging NADH in live cells *in vitro*. Polyfluorene Pdots with ultrabright fluorescence have been applied previously to cell labeling.[47] Of the polyfluorene Pdots tested, the PFBT Pdots exhibited the highest NADH sensitivity; therefore, we selected these Pdots for *in vitro* experiments. PFBT Pdots were functionalized with streptavidin to target biotinylated anti-EpCAM antibodies bound to EpCAM on the surface of MCF-7 breast-cancer cells (Figure S8).[48] Pdot-labeled MCF-7 cells showed a large decrease in fluorescence intensity in the presence of 1 mM NADH in PBS versus without NADH (Figure S9), indicating NADH detection.

Imaging NADH in vivo

We next tested whether the effect of NADH on the emission of DPN-CNPPV Pdots could be exploited to allow ratiometric imaging of NADH *in vivo* using a smartphone with RGB image analysis. DPA-CNPPV Pdots exhibit a fluorescence color shift from red to blue when exposed to physiological concentrations of NADH (Figure 4a). True-color images collected with a smartphone can be split into red (R), green (G), and blue (B) channels and digitized using an image-processing algorithm, and the ratio of blue- and red-channel intensities (B/R ratio) can be used to quantify NADH concentration (Figure 4b). Figure 4c shows the linear response of the B/R ratio to NADH concentration over the physiological range of 0–2 mM. The enhancement in B/R ratio is over 100-fold between 0 and 2 mM NADH (Figure 4d–f). The sensitivity is higher than when directly testing NADH fluorescence with a smartphone (Figure S10).

The feasibility of using DPA-CNPPV Pdots for ratiometric imaging of NADH *in vivo* was tested by subcutaneously injecting DPA-CNPPV Pdots in PBS together with different concentrations of NADH (at 0 mM, i.e. no NADH, and at 0.25, 0.5, and 1.0 mM NADH) into the dorsal area of nude mice. UV lamp was used for illumination and a smartphone camera for imaging (Figure 4g). Figure 4h shows the concentration-dependent sensing at the various NADH concentrations (0.25, 0.5, and 1.0 mM). True-color images of regions of interest were split into blue- and red-channel images to calculate the B/R ratio (Figure 4i, j). The B/R ratio showed excellent linearity in the Pdot sensor's *in vivo* NADH detection response.

Conclusions

In this study we explored a series of fluorescent NADH-sensitive Pdots for use as NADH nanoprobes, and identified DPA-CNPPV Pdots as a promising reversible ratiometric NADH sensor. All Pdots characterized showed excellent brightness and photostability; the ratiometric DPA-CNPPV Pdot exhibited superior NADH sensitivity and selectivity, and a fast and reversible response. We demonstrate the feasibility of point-of-care use by performing ratiometric imaging of NADH *in vivo* using the DPA-CNPPV Pdots with a smartphone and simple RGB image processing.

Supplementary Material

Refer to Web version on PubMed Central for supplementary material.

Acknowledgements

This research was supported by the University of Washington and the National Institutes of Health (R01MH113333) (D.T.C.), and by the Shenzhen Science and Technology Innovation Commission (Grant No. KQTD20170810111314625), the National Natural Science Foundation of China (Grant No. 81771930), and the National Key R&D Program of China (Grant No. 2020YFA0909000, 2018YFB0407200) (C.W.).

References

[1]. Zhao Y, Yang Y, Free Radicals Biol. Med 2016, 100, 43–52.

[2]. Popov VO, Lamzin VS, Biochem. J 1994, 301, 625. [PubMed: 8053888]

[3]. Zhao Y, Wang A, Zou Y, Su N, Loscalzo J, Yang Y, Nat. Protoc 2016, 11, 1345. [PubMed: 27362337]

[4]. Wiederkehr A, Demaurex N, Nat. Methods 2017, 14, 671. [PubMed: 28661497]

[5]. Eto K, Tsubamoto Y, Terauchi Y, Sugiyama T, Kishimoto T, Takahashi N, Yamauchi N, Kubota N, Murayama S, Aizawa T, Science 1999, 283, 981–985. [PubMed: 9974390]

[6]. Cameron WD, Bui CV, Hutchinson A, Loppnau P, Gräslund S, Rocheleau JV, Nat. Methods 2016, 13, 352. [PubMed: 26878383]

[7]. Ying W, Antioxid. Redox Signaling 2008, 10, 179–206.

[8]. Lin S-J, Guarente L, Curr. Opin. Cell Biol 2003, 15, 241–246. [PubMed: 12648681]

[9]. Ying W, Front. Biosci2007, 12, 1863–1888. [PubMed: 17127427]

[10]. Omar FS, Duraisamy N, Ramesh K, Ramesh S, Biosens. Bioelectron 2016, 79, 763–775. [PubMed: 26774092]

[11]. Yaseen MA, Sakadžić S, Wu W, Becker W, Kasischke KA, Boas DA, Biomed. Opt. Express 2013, 4, 307–321. [PubMed: 23412419]

[12]. S Thrane A, Takano T, Thrane VR, Wang F, Peng W, Ottersen OP, Nedergaard M, A Nagelhus E, Cereb J. Blood Flow Metab. 2013, 33, 996–999.

[13]. Vergen J, Hecht C, Zholudeva LV, Marquardt MM, Hallworth R, Nichols MG, Microsc. Microanal 2012, 18, 761–770. [PubMed: 22832200]

[14]. Wu C, Chiu DT, Angew. Chem. Int. Ed 2013, 52, 3086–3109.

[15]. Li J, Pu K, Chem. Soc. Rev 2019, 48, 38–71. [PubMed: 30387803]

[16]. Guo B, Chen J, Chen N, Middha E, Xu S, Pan Y, Wu M, Li K, Liu C, Liu B, Adv. Mater 2019, 31, 1808355.

[17]. Zhang B, Wang F, Zhou H, Gao D, Yuan Z, Wu C, Zhang X, Angew. Chem. Int. Ed 2019, 58, 2744–2748.

[18]. Feng L, Zhu C, Yuan H, Liu L, Lv F, Wang S, Chem. Soc. Rev 2013, 42, 6620–6633. [PubMed: 23744297]

[19]. Jiang Y, McNeill J, Chem. Rev 2016, 117, 838–859. [PubMed: 28029769]

[20]. Miao Q, Xie C, Zhen X, Lyu Y, Duan H, Liu X, Jokerst JV, Pu K, Nat. Biotechnol 2017, 35, 1102. [PubMed: 29035373]

[21]. Pu K, Shuhendler AJ, Jokerst JV, Mei J, Gambhir SS, Bao Z, Rao J, Nat. Nanotechnol 2014, 9, 233. [PubMed: 24463363]

[22]. Wu C, Jin Y, Schneider T, Burnham DR, Smith PB, Chiu DT, Angew. Chem. Int. Ed 2010, 49, 9436–9440.

[23]. Cui D, Li J, Zhao X, Pu K, Zhang R, Adv. Mater 2020, 6, 1906314.

[24]. Ke C-S, Fang C-C, Yan J-Y, Tseng P-J, Pyle JR, Chen C-P, Lin S-Y, Chen J, Zhang X, Chan Y-H, ACS Nano 2017, 11, 3166–3177. [PubMed: 28221751]

[25]. Yu J, Wu C, Sahu SP, Fernando LP, Szymanski C, McNeill J, J. Am. Chem. Soc 2009, 131, 18410–18414. [PubMed: 20028148]

[26]. Chen H, Fang X, Jin Y, Hu X, Yin M, Men X, Chen N, Fan C, Chiu DT, Wan Y, Small 2018, 14, 1800239.

[27]. Li J, Cui D, Jiang Y, Huang J, Cheng P, Pu K, Adv. Mater 2019, 31, 1905091.

[28]. Sun K, Li S, Li Q, Tang Y, Qin W, Yu J, Chiu DT, Yuan Z, Zhang X, Wu C, ACS Nano 2016, 10, 6769–6781. [PubMed: 27303785]

[29]. Wu L, Wu I, DuFort CC, Carlson MA, Wu X, Chen L, Kuo CT, Qing Y, Yu J, Hingorani SR, Chiu DT, J. Amer. Chem. Soc 2017, 139, 6911–6918. [PubMed: 28459559]

[30]. Chan Y-H, Wu C, Ye F, Jin Y, Smith PB, Chiu DT, Anal. Chem 2011, 83, 1448–1455. [PubMed: 21244093]

[31]. Ding Z, Dou X, Wang C, Feng G, Xie J, Zhang X, Nanotechnology 2021, DOI: 10.1088/1361-6528/abea38.

[32]. Ye F, Wu C, Jin Y, Chan Y-H, Zhang X, Chiu DT, J. Am. Chem. Soc 2011, 133, 8146–8149. [PubMed: 21548583]

[33]. Chan Y-H, Jin Y, Wu C, Chiu DT, Chem. Commun 2011, 47, 2820–2822.

[34]. Shi H, Ma X, Zhao Q, Liu B, Qu Q, An Z, Zhao Y, Huang W, Adv. Funct. Mater 2014, 24, 4823–4830.

[35]. Sun K, Yang Y, Zhou H, Yin S, Qin W, Yu J, Chiu DT, Yuan Z, Zhang X, Wu C, ACS Nano 2018, 12, 5176–5184. [PubMed: 29694016]

[36]. Sun K, Ding Z, Zhang J, Chen H, Qin Y, Xu S, Wu C, Yu J, Chiu DT, Adv. Healthcare Materials, 2020, 10, 2001019.

[37]. Lyu Y, Cui D, Huang J, Fan W, Miao Y, Pu K, Angew. Chem. Int. Ed 2019, 58, 4983–4987.

[38]. Higgins DS Jr, Greenamyre JT, J. Neurosci 1996, 16, 3807–3816. [PubMed: 8656275]

[39]. Titov DV, Cracan V, Goodman RP, Peng J, Grabarek Z, Mootha VK, Science 2016, 352, 231–235. [PubMed: 27124460]

[40]. Gesquiere AJ, Park S-J, Barbara PF, J. Am. Chem. Soc 2005, 127, 9556–9560. [PubMed: 15984882]

[41]. Yu J, Wu C, Tian Z, McNeill J, Nano Lett. 2012, 12, 1300–1306. [PubMed: 22313320]

[42]. Huang X, Song J, Yung BC, Huang X, Xiong Y, Chen X, Chem. Soc. Rev 2018, 47, 2873–2920. [PubMed: 29568836]

[43]. Wu L, Wu I-C, DuFort CC, Carlson MA, Wu X, Chen L, Kuo C-T, Qin Y, Yu J, Hingorani SR, J. Am. Chem. Soc 2017, 139, 6911–6918. [PubMed: 28459559]

[44]. Li Q, Sun K, Chang K, Yu J, Chiu DT, Wu C, Qin W, Anal. Chem 2013, 85, 9087–9091. [PubMed: 23964730]

[45]. Hustad S, C McKinley M, McNulty H, Schneede J, Strain J, M Scott J, Ueland PM, Clin. Chem 2002, 48, 1571–1577. [PubMed: 12194936]

[46]. Fabian E, Majchrzak D, Dieminger B, Meyer E, Elmadfa I, Ann. Nutr. Metab 2008, 52, 29–36.

[47]. Wu C, Bull B, Szymanski C, Christensen K, McNeill J, ACS Nano 2008, 2, 2415–2423. [PubMed: 19206410]

[48]. Wu C, Schneider T, Zeigler M, Yu J, Schiro PG, Burnham DR, McNeill JD, Chiu DT, J. Am. Chem. Soc 2010, 132, 15410–15417. [PubMed: 20929226]

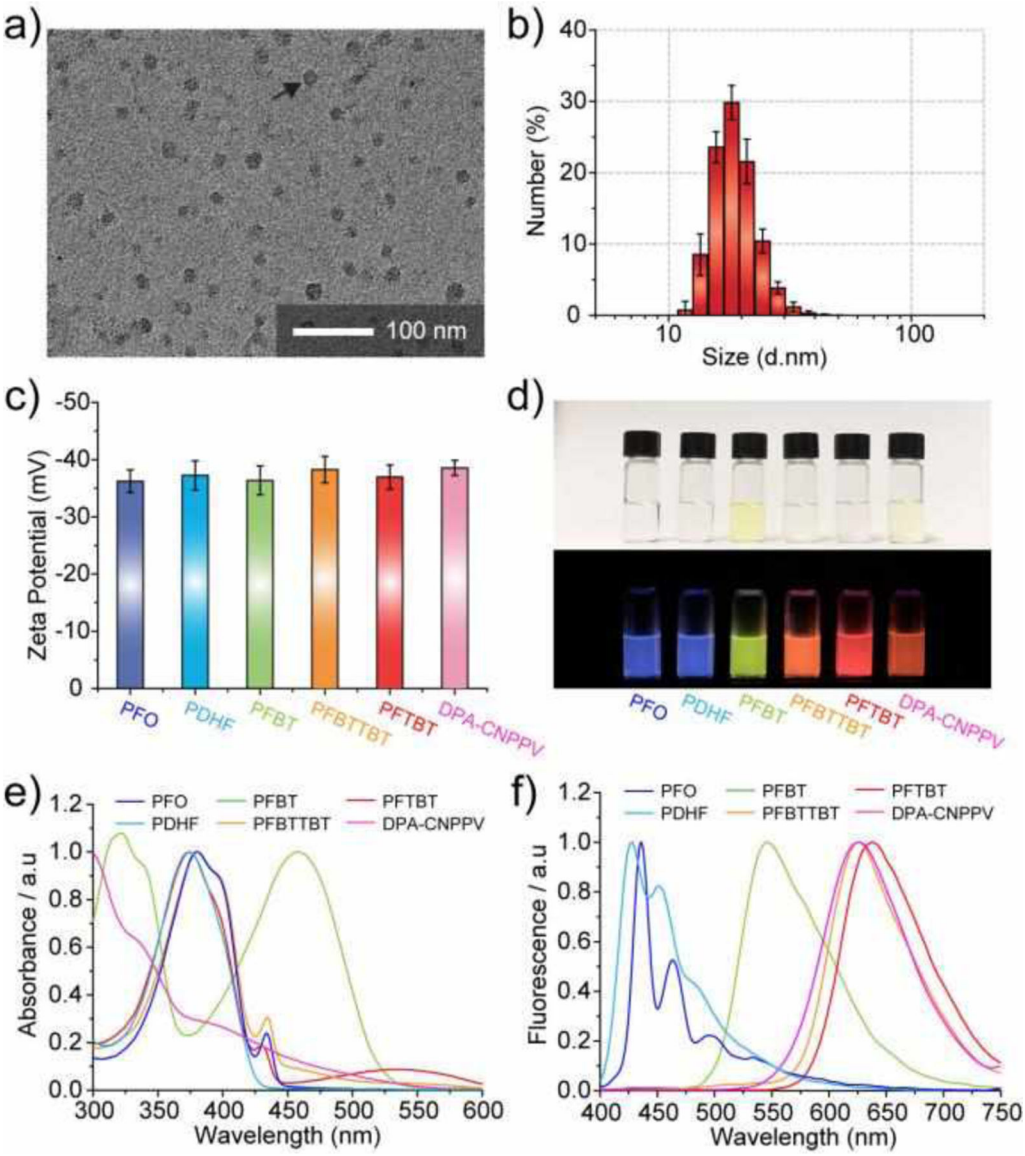

Figure 1. Characterization of Pdots.

(a) TEM image of PFBT Pdots. (b) Size distribution of PFBT Pdots based on DLS measurements. (c) Zeta potentials of six Pdots. (d) Photographs of Pdot suspensions illuminated by ambient indoor light (upper) and UV light (365 nm; lower). Pdot emissions are intense and span the visible spectrum. (e) Absorption spectra. (f) Emission spectra (λ_{ex} = 365 nm

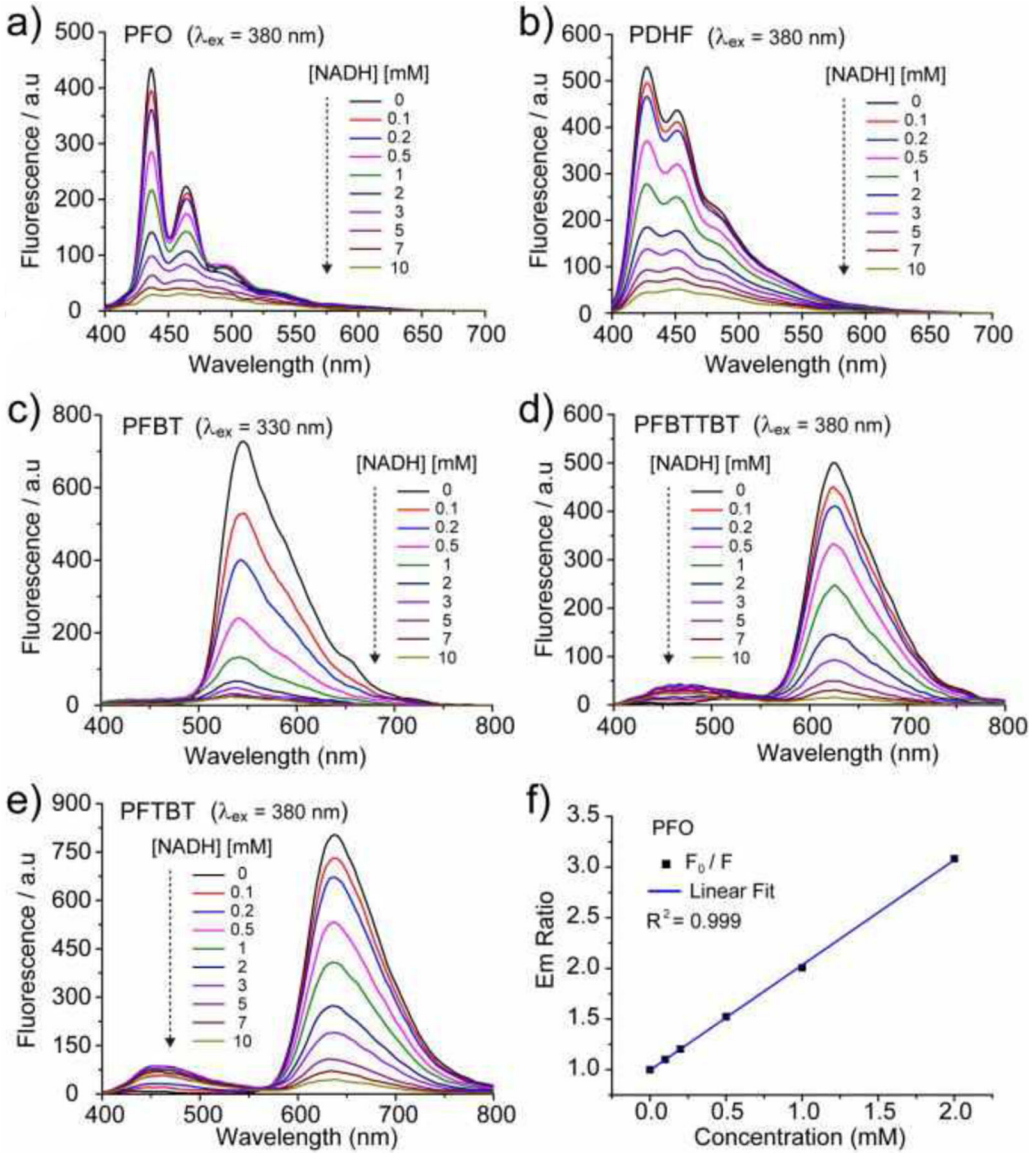

Figure 2. Fluorescence response of polyfluorene Pdots to NADH.

(a–e) Emission spectra of polyfluorene Pdots at 0–10 mM NADH with excitation of the fluorene group (λ_{ex} = 330 or 380 nm). Pdot emission intensity decreases with increasing NADH. (f) Stern-Volmer plot for PFO Pdots showing the ratio of fluorescence emission intensity at 428 nm in the absence (F_0) and presence (F) of NADH at various NADH concentrations (λ_{em} = 436 nm). F_0/F showed a linear relationship with NADH concentration over the physiological range of 0–2 mM NADH.

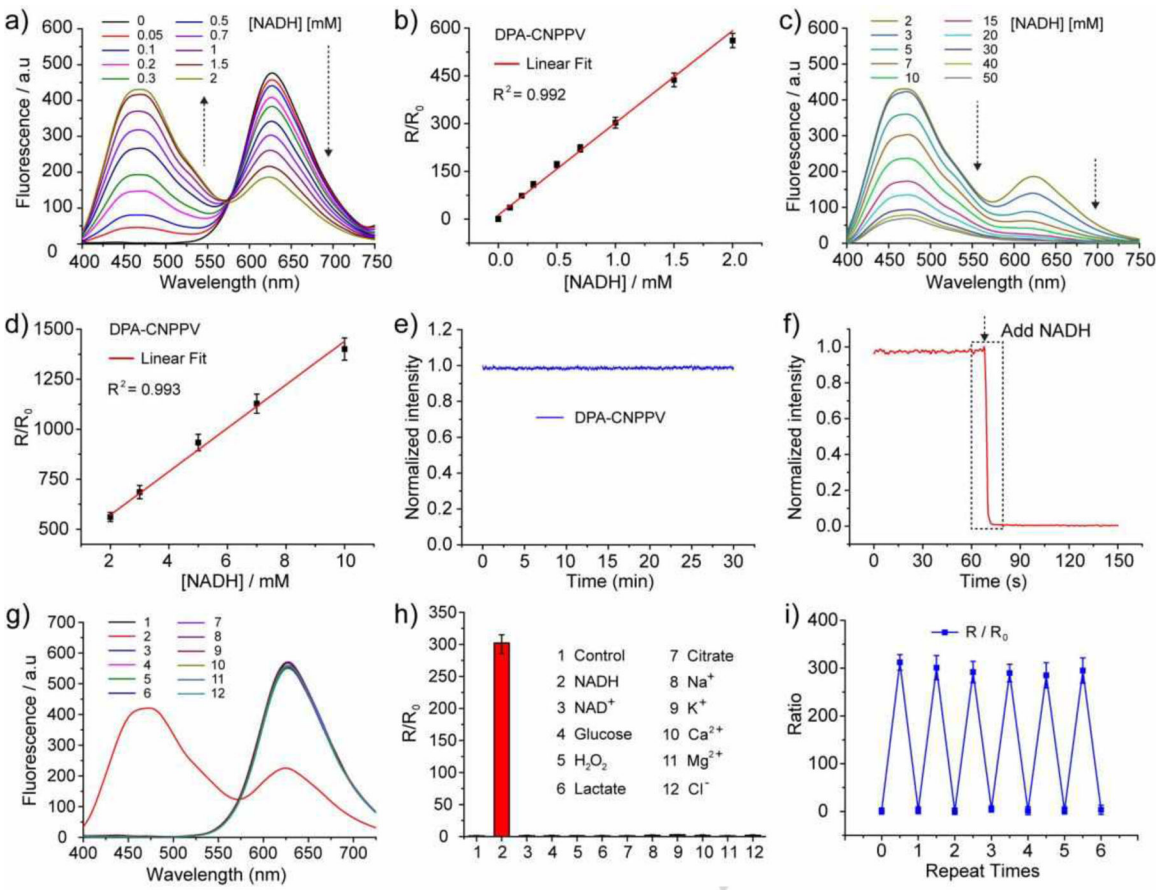

Figure 3. Reversible ratiometric NADH sensing using DPA-CNPPV Pdots.

(a) Emission spectra of DPA-CNPPV Pdots (0.02 mg/mL) at 0–2 mM NADH with excitation at 385 nm. (b) Ratiometric calibration curve, calculated using data shown in panel a. $R = I_{458nm}/I_{627nm}$; R_0 = R in the absence of NADH. (c) Emission spectra of DPA-CNPPV Pdots at 2–50 mM NADH, and (d) corresponding ratiometric calibration curve. (e) Photostability of DPA-CNPPV Pdots indicated by consistent emission at 627 nm for 30 min with excitation at 385 nm. (f) Rapid response (<5 s) of DPA-CNPPV Pdots to addition of 1 mM NADH. (g) Emission spectra of DPA-CNPPV Pdots in the presence of NADH (red curve), 10 other analytes, and a PBS control, demonstrating the specificity of the response to NADH. Numbers 1–12 are defined in panel h. (h) Selectivity of DPA-CNPPV Pdot response to NADH versus 10 other biological analytes at 1 mM. R/R_0 values were calculated based on the spectra shown in panel g. Only NADH (red bar) produced a significant fluorescence response. (i) Reversibility of response of DPA-CNPPV Pdots to repeated exposure to 0 and 1 mM NADH DPA by using ultrafiltration and gel filtration.

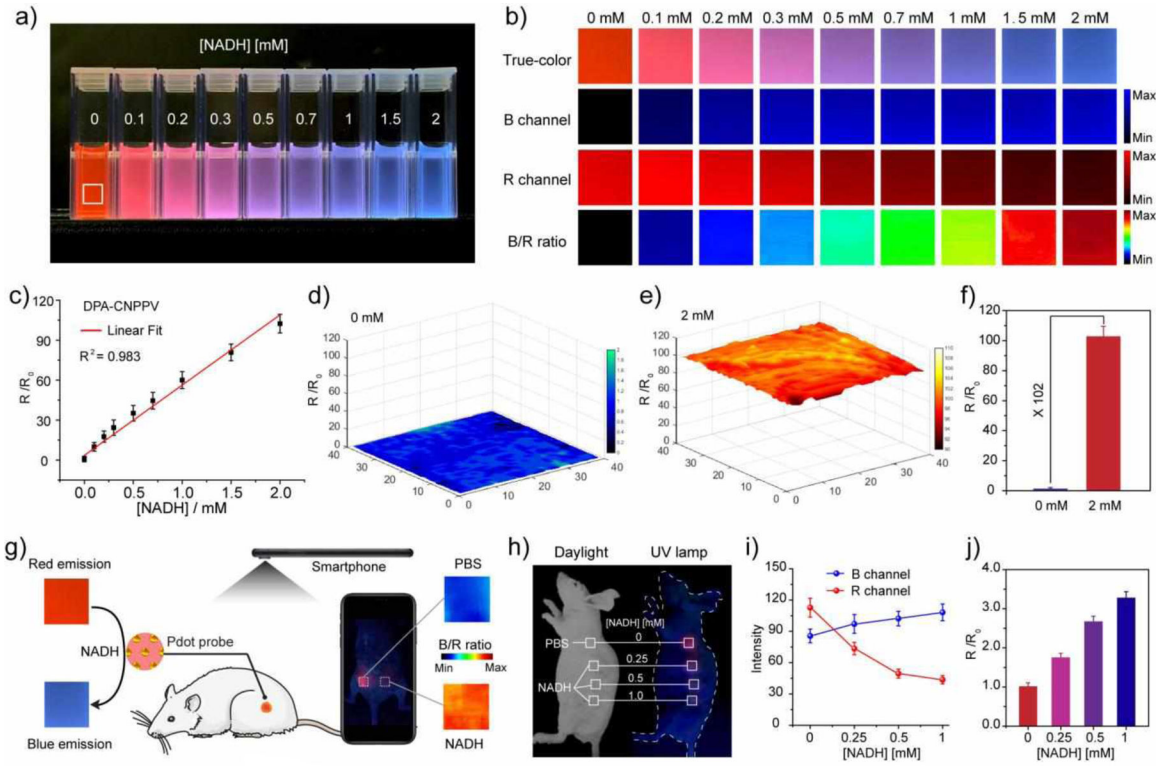

Figure 4. Image processing algorithm for ratiometric imaging of NADH *in vivo*.

(a) DPA-CNPPV Pdots at different NADH concentrations from 0 to 2 mM with illumination at 365 nm. (b) True-color images are split into RGB channels, and the B/R ratio is calculated from pixearrays of the B and R channels. (c) Ratiometric calibration curve of DPA-CNPPV Pdots at 0–2 mM NADH. (d, e) 3D distribution and (f) mean R/R_0 at 0 and 2 mM NADH. (g) Ratiometric imaging of NADH *in vivo* with DPA-CNPPV Pdots and a smartphone. Emission shifts from red to blue as NADH concentration increases. Pdots were injected into mice at two locations, with and without NADH (0.1 μmol). Heatmap images of the ratio of blue- and red-channel intensities (B/R ratio) from the two injection regions are shown on the right. High B/R ratio (red) indicates high NADH concentration. (h) Concentration-dependent ratiometric imaging of NADH in live mice with a smartphone camera. The regions of interest (square-marked area) correspond to locations of subcutaneous injections of DPA-CNPPV Pdots either alone (0.1 mg/mL, 100 μL; 0 mM NADH) or together with NADH (0.25, 0.5, and 1.0 mM). (i) Fluorescence intensities of the B and R channels. (j) Mean R/R_0 for the regions of interest.

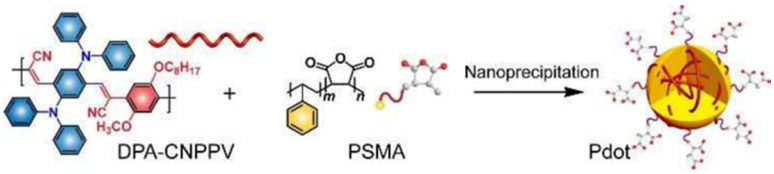

Scheme 1. Pdot preparation.

Pdots were synthesized by nanoprecipitation of a fluorescent semiconducting polymer (DPA-CNPPV is shown here) and the amphiphilic polymer PSMA.

Table 1.

Pdot photophysical properties.

Pdot	λ_{max}^{abs} (nm)[a]	λ_{max}^{em} (nm)[b]	Size (nm)[c]	ζ (mV)[d]	LOD (μM)[e]	K_{SV} (M^{-1})[f]
PFO	380	436	20.2±1.5	−36.2	25	1.04×10^3
PDHF	374	428	22.1±1.8	−37.2	36	0.94×10^3
PFBT	322, 458	546	19.3±1.9	−36.4	14	4.89×10^3
PFBTTBT	380	626	19.7±1.4	−38.2	27	1.17×10^3
PFTBT	374, 528	638	17.5±2.2	−36.9	28	0.97×10^3
DPA-CNPPV	294	627	18.8±1.8	−38.5	3.1	N.A.

[a] Absorption maximum.

[b] Emission maximum.

[c] Average hydrodynamic diameter based on DLS measurements (n=5).

[d] Zeta potential.

[e] Limit of detection ([NADH]).

[f] Quenching constant (0–2 mM NADH).